Journal of Macromolecular Science, Part A
Publication details, including instructions for authors and subscription information:
http://www.informaworld.com/smpp/title~content=t713597274

Small-Angle Neutron Scattering Studies of Polymers: Selected Aspects

R. W. Richards[a]
[a] Department of Pure and Applied Chemistry, University of Strathclyde, Glasgow, United Kingdom

To cite this Article Richards, R. W.(1989) 'Small-Angle Neutron Scattering Studies of Polymers: Selected Aspects', Journal of Macromolecular Science, Part A, 26: 5, 787 — 815
To link to this Article: DOI: 10.1080/00222338908052011
URL: http://dx.doi.org/10.1080/00222338908052011

J. MACROMOL. SCI.–CHEM., A26(5), pp. 787-815 (1989)

SMALL-ANGLE NEUTRON SCATTERING STUDIES OF POLYMERS: SELECTED ASPECTS

R. W. RICHARDS

Department of Pure and Applied Chemistry
University of Strathclyde
Glasgow, United Kingdom G1 1XL

INTRODUCTION

Small-angle neutron scattering (SANS) studies of polymers are no longer a rarity in polymer science. It is now widely appreciated that SANS can provide unique data which provide greater insight into polymer structural properties than otherwise obtainable. Nonetheless, the costs of the apparatus and special efforts that have to be taken to prepare necessary deuterated polymers mean that such experiments have to be designed with care to ensure that unambiguous data are obtained. There are now in existence several reviews on various aspects [1-4] of SANS studies of polymers; attention in this review is focused on multiphase polymer systems. However, newer aspects of SANS studies on homopolymers will also be discussed, and we begin by a necessarily brief survey of the relevant theoretical expressions.

THEORY

Detailed expositions of the general theory of neutron scattering have been provided by Marshall and Lovesey [5] and by Lovesey [6], while a fuller and wider discussion of SANS as a general technique in materials science is available in the book by Kostorz [7].

The angular variation of the intensity of neutrons scattered by a material on which a neutron beam of intensity I_0 (neutrons$\cdot$cm$^{-2}\cdot$s^{-1}) impinges is given by

$$I(Q) = CI_0(d\sigma/d\Omega), \tag{1}$$

where C is an instrumental factor depending on the geometry of sample-detector layout, $d\sigma/d\Omega$ is the differential scattering cross section, and Q is the scattering vector, i.e., $(4\pi/\lambda)\sin\theta$, where λ is the wavelength of the neutron beam and 2θ is the scattering angle (i.e., the angle between the incident beam direction and the line connecting the detector to the center of the scattering volume).

The differential scattering cross section has two components: a coherent scattering cross section, $(d\sigma/d\Omega)_{coh}$, and an incoherent scattering cross section, $\Sigma_I/4\pi$. The former of these retains all the phase information of the scattering process and hence has all the structural information. The coherent component has no structural information (but much information on dynamic processes) and is a troublesome background or "noise" component of the total signal. For a two-phase model for the scattering substance, i.e., N_p particles embedded in a continuous matrix,

$$I(Q) = F(N_p(d\sigma/d\Omega)_{coh} + \Sigma_I/4\pi), \tag{2}$$

where F is a factor incorporating the incident neutron flux and the geometrical characteristics of the instrument. Taking this model further, we have

$$I(Q) = F[N_p V_p^2(\rho_p - \rho_m)^2 S(Q) + \Sigma_I/4\pi], \tag{3}$$

where V_p is the scattering particle volume, $S(Q)$ is the scattering law for the system, and ρ_p and ρ_m are the scattering length densities of the particle and matrix, respectively.

The factor $(\rho_p - \rho_m)$ is often called the contrast factor, K. Clearly, to obtain the best quality scattering data possible from Eq. (3) we need to maximize K and minimize Σ_I to ensure that the coherent scattering component does not become buried. The contrast factor is generated by incorporating a known proportion of deuterated polymer into an identical (in terms of molecular weight, tacticity, molecular weight distribution, etc.) hydrogenous polymer. Values of ρ and Σ_I can be calculated from known values of the scattering length and incoherent scattering cross section for the atoms that make up the monomer unit of the polymer chain. Table 1 lists values of these two parameters for common elements in polymers.

The calculation of the scattering length density and incoherent scattering cross section for the monomer units is equivalent to identifying these units as point scatterers over which the scattered intensity is averaged. We then have

$$\rho = N_A d \Sigma b_i / M,$$

$$\Sigma_I = N_A d \Sigma \sigma_i / M,$$

where N_A is Avogadro's number, d is the polymer density, M is the molar mass of the monomer unit, and the summations extend over all atomic species in the monomer units. For studies of polymers by SANS, the most significant values of the scattering length are those for hydrogen and deuterium. Replacement of the hydrogen atoms in a polymer by deuterium changes the scattering length density considerably, and a significant contrast factor is developed. Values of the scattering length density and incoherent scattering cross section are given in Table 2 for some common polymers and solvents.

Since the contrast factor appears as a squared term in Eq. (3), we are at liberty to disperse hydrogenous polymer in a deuterated matrix to generate contrast rather than the other way round. This has often been done for polymers dissolved in low molecular weight solvents and has the added advantage that the incoherent background is very low under these circumstances. For polymers in the solid state, this technique is not so successful. Generally, solid plaques of polymers, especially if compression molded, contain microvoids. These microvoids generate a very large contrast in a deuterated matrix and produces a strongly Q-dependent scattering, which corrupts the desired molecular scattering in a manner from which it cannot be deconvoluted.

TABLE 1. Coherent Scattering Lengths and Incoherent Scattering Cross Section

Nucleus	Coherent scattering length, b, 10^{-10} cm	Incoherent scattering cross section, σ_i, 10^{-24} cm^2
^{1}H	-0.374	79.9
^{2}H	0.667	2.0
^{12}C	0.665	0
^{14}N	0.937	0.49
^{16}O	0.580	0
^{28}Si	0.411	0.01
^{35}Cl	1.160	5.2

TABLE 2. Scattering Length Densities and Macroscopic Incoherent Scattering Cross Sections for Selected Polymers and Solvents

Polymer/solvent	Scattering-length density, ρ, 10^{10} cm^{-2}	Incoherent scattering cross section, $\Sigma_I/4\pi$, cm^2
Polyethylene	-0.34	6.86
Polyethylene-d4	8.24	0.15
Polystyrene	1.41	3.69
Polystyrene-d8	6.3	0.08_6
Polybutadiene	0.47	5.33
Polybutadiene-d6	6.82	0.12
Water	-0.56	5.32
Water-d2	6.36	0.12
Toluene	0.94	4.18
Toluene-d8	5.42	0.09_8

When a hydrogenous matrix is used, the incoherent background scattering is much larger, but *flat*, and the scattering from the voids is subsumed into it with the stronger molecular scattering superimposed onto the background.

SCATTERING LAWS

The form of the scattering law in Eq. (3) depends on the arrangement of the scattering centers with respect to each other. More precisely, the scattering law is the Fourier transform of the density correlation function describing the scattering length density distribution in the scattering system. Many scattering laws have been derived for various types of molecules or regularly shaped bodies and are available in the literature [8]. Debye [9] derived an expression for the scattering law of a Gaussian coil which is perhaps the most generally useful to describe the molecular scattering of polymer molecules:

$$S(Q) = 2/u^2\,[\exp(-u) - 1 + u],$$
$$u = Q^2\langle S^2\rangle, \tag{4}$$

where $\langle S^2 \rangle$ is the mean-square radius of gyration (z-average) of the molecule.

Figure 1 shows the form of this scattering law, but the different regions become more apparent in the Kratky plot of Fig. 2. Where $Q\langle S^2 \rangle^{1/2}$ is greater than unity, the intensity has a Q^{-2} dependence and $Q^2\langle S^2 \rangle I(Q)$ asymptotically approaches a plateau value of 2. In reality, there are deviations from this plateau behavior which give valuable information on the short-range order in polymer chains. Examples of this will be discussed later.

Commonly, the region where $\langle S^2 \rangle^{1/2}$ is equal to or less than unity is called the Guinier region, and it is in this range that scattering data can be used to obtain the radius of gyration of a polymer molecule in the solid state or in solution. If the polymer is monodisperse with respect to molecular weight, this Guinier condition must be strictly observed. For broader molecular weight distributions, Ullman [10] has shown that this condition can be relaxed. For $Q\langle S^2 \rangle^{1/2}$ less than unity, the exponential in Eq. (4) can be expanded and simplification gives

$$S(Q) = (1 - Q^2\langle S^2 \rangle/3). \tag{5}$$

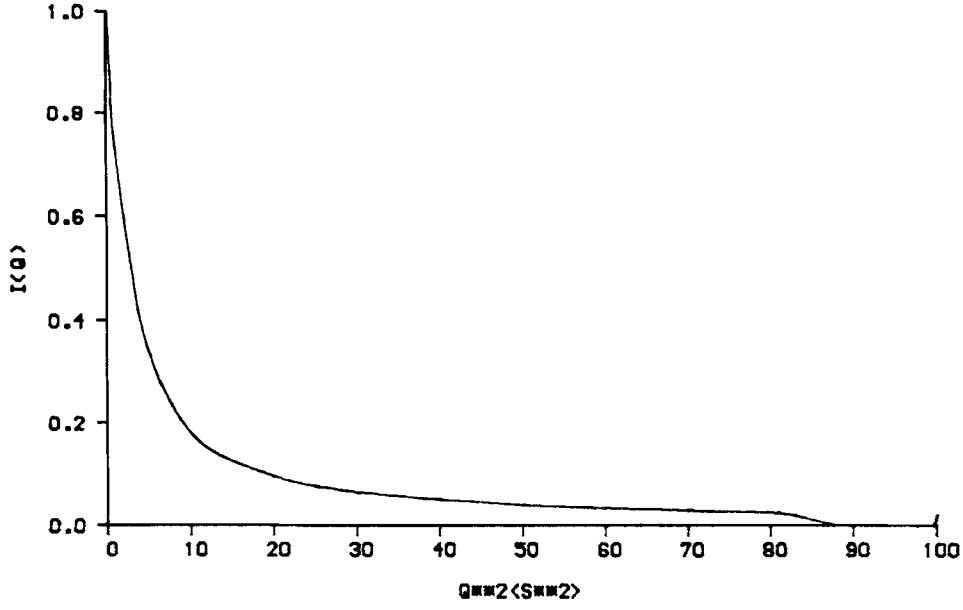

FIG. 1. Predicted scattering from Eq. (4) as a function of the dimensionless variable $Q^2\langle S^2 \rangle$.

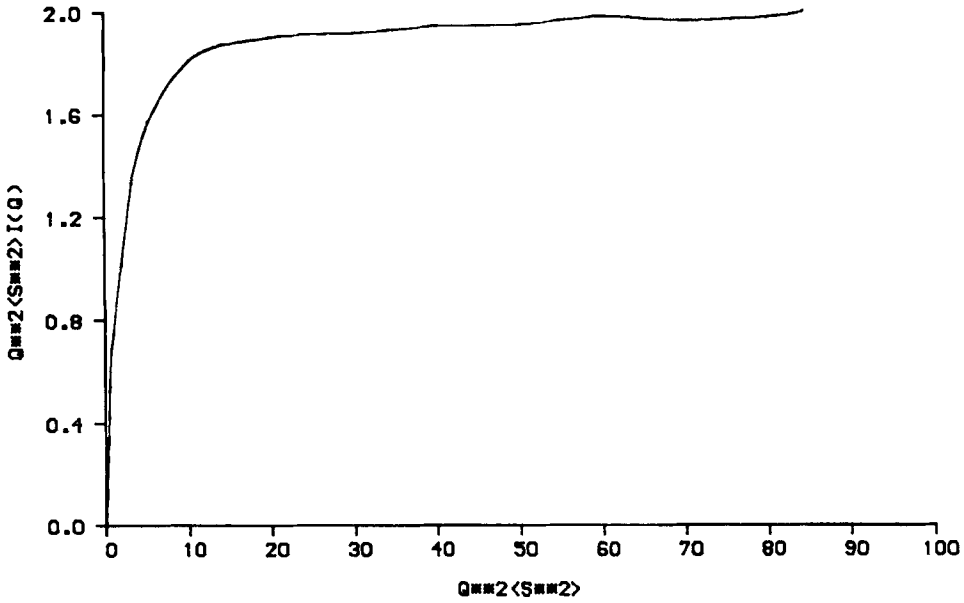

FIG. 2. Kratky plot of the data of Fig. 1 in dimensionless form.

Rayleigh [11] derived the scattering law for a solid sphere many years ago:

$$S(Q) = [3/(QR)^3(\sin QR - QR \cos QR)]^2, \quad (6)$$

where R is the radius of the sphere. The form of this equation is shown in Fig. 3, together with the scattering laws for cylinders and lamellae. It is not surprising that these bodies of very different morphology should have similar scattering laws; they each contain a Bessel function as the kernel of the scattering law. For low values of QR (i.e., $QR < 1$) and expansion of the sine and cosine terms in Eq. (6), it is easy to show by equating Eqs. (5) and (6) that the mean-square radius of gyration of a sphere is $(3/5)R^2$.

STATISTICAL DESCRIPTION OF SCATTERING

Where the application of models such as those outlined above to scattering data may not be valid, recourse may be made to a statistical description of the

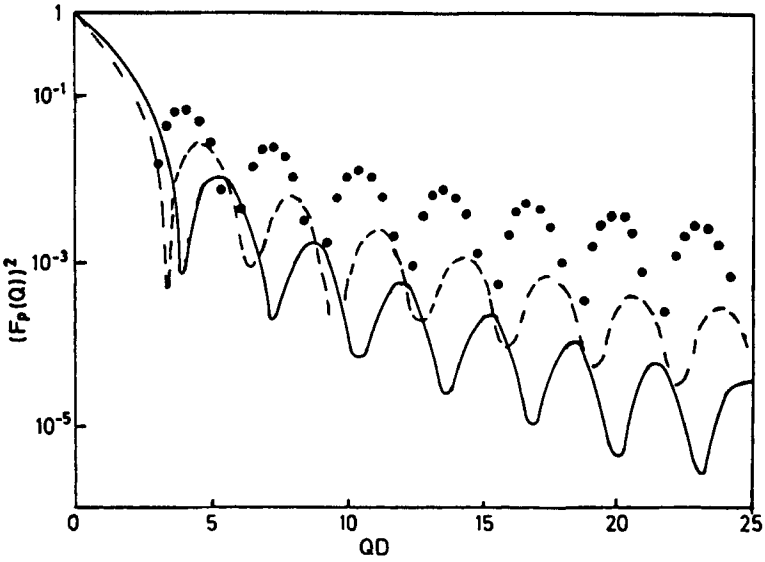

FIG. 3. Scattering laws from solid spheres (——), cylinders (– –), and lamellae (●●).

scattering. The variation of density within a system is described by a correlation function [12], $\gamma(r)$, and we have

$$S(Q) = 4\pi\langle\eta^2\rangle \int_0^\infty \gamma(r)(\sin Qr/Qr)r^2\, dr, \tag{7}$$

where $\langle \eta^2 \rangle$ is the mean square fluctuation of scattering length density. Fourier transforming of Eq. (7) gives

$$\gamma(r) = \langle \eta^2 \rangle / 2\pi \int_0^\infty S(Q)(\sin Qr/Qr)Q^2\, dQ.$$

From the properties of the correlation function namely, $\gamma(r) = 1$ at $r = 0$ and $\gamma(r) = 0$ at $r = 0$, we can define an expression for $\langle \eta^2 \rangle$:

$$\langle \eta^2 \rangle = 2\pi / \int_0^\infty S(Q)Q^2\, dQ,$$

and thus

$$\gamma(r) = \frac{\int_0^\infty S(Q)(\sin Qr/Qr)Q^2\, dQ}{\int_0^\infty S(Q)Q^2\, dQ}. \tag{8}$$

The major practical difficulty with this approach is that, rigorously, the integrations in Eq. (8) have to be performed from $Q = 0$ to $Q = \infty$. These limits can never be attained, of course, but application of the statistical method does necessitate collection of SANS data over as wide a Q range as possible, and limiting the integral to the range of Q values used. This necessarily truncates the correlation function but introduces no artifacts. The range of real space values, r, over which $\gamma(r)$ is defined is then

$$2\pi/Q_{max} \leqslant r \leqslant 2\pi/Q_{min}.$$

From the correlation function, a value for the correlation length, a_c, can be obtained:

$$a_c = 2\int_0^\infty \gamma(r)\, dr. \tag{9}$$

Here again the integration has to be confined to the range of r values probed by the SANS experiment. For a two-phase system, the Porod chord length in Phase 1 (l_1) is the mean distance traversed through that phase by an infinite number of straight lines drawn at random through the material. Hence,

$$l_1 = a_c/\phi_2 \quad \text{and} \quad l_2 = a_c/(1 - \phi_2).$$

For a solid sphere of radius R, the correlation function is given by

$$\gamma(r) = 1 - (3/4)r/R + (1/16)(r/R)^3. \tag{10}$$

BLOCK COPOLYMERS MICROPHASE STRUCTURE

A considerable amount of SANS [13] work has been done on styrene-diene block copolymers. Little of it has been concerned with molecular dimensions in the domains. The majority of the work has been concerned

with evaluation of the domain size, separation and organization of the domains, and comparison of the data with the statistical thermodynamic theory of Helfand [14]. As is well known, styrene-diene block copolymers have a microphase-separated solid state with domains of regular morphology of the minor component dispersed in an ordered manner throughout the matrix of the major component. The domain morphology depends on the copolymer composition. As the weight fraction of minor components increases, the initially spherical domains become cylindrical, and then an alternating lamellar structure prevails at weight fractions between 0.4 to 0.6. Helfand and coworkers developed an equilibrium statistical thermodynamic theory of domain size (radius or half thickness of the lamellae) and separation. This resulted from the minimization of the free-energy equation for the formation of the microphase-separated state. The minimization was aided by invoking a narrow interphase approximation, i.e., the region over which the density smoothly changes from that of one phase to the other is very much less than the distance separating the domains. The theory predicts that

$$D \propto M_D^{0.67} \tag{11}$$

and

$$d \propto M^{0.67}, \tag{12}$$

where D is the characteristic dimension of the domain and d is the distance between domains, while M_D and M are the molecular weights of the domain-forming block and the whole copolymer molecule, respectively.

In styrene-diene block copolymers the regularity of the arrangement of the domains with respect to each other means that the scattering law has a contribution in addition to that describing an isolated domain:

$$S(Q) = P(Q)\, A(Q),$$

where $P(Q)$ is the scattering law for an isolated domain, e.g., Eq. (6), and $A(Q)$ is the interference function scattering law descriptive of the arrangement of domains with respect to each other.

Figure 4 shows experimental SANS data obtained for a styrene-isoprene diblock copolymer. The interference function scattering is apparent in the very intense Bragg peaks at Q values of ~0.007 and 0.01 $Å^{-1}$; a third Bragg peak has overlapped with one of the maxima of the $P(Q)$ function at ~0.013 $Å^{-1}$. At higher values of Q only the broad maxima of $P(Q)$ are apparent.

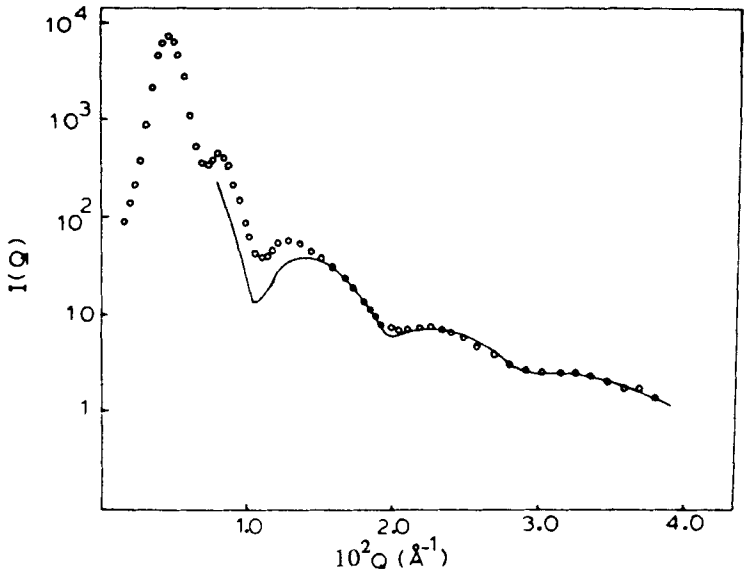

FIG. 4. Small-angle neutron scattering profile form a hydrogenous styrene-isoprene diblock copolymer. Styrene weight fraction 0.85, molecular weight 292 500.

When the copolymer is synthesized with fully deuterated styrene blocks, the $P(Q)$ are evident to much higher values of Q (Fig. 5) where the interference function, $A(Q)$, has a value of 1. From the Q value of the first peak (Q_1), the spacing between domains can be calculated as $2\pi/Q_1$. The arrangement of the domains may be inferred from the ratio of this spacing to that calculated from the higher-order Bragg peaks. This is straightforward for lamellar domains, and it is not too difficult even for cylindrical domains.

For spherical domains the unambiguous assignment of domain arrangement is not possible. Cylindrical domains are arranged on a hexagonal lattice, and although it is clear that spherical domains are on a cubic lattice, there is insufficient resolution of the scattering data to be able to decide between a face-centered cubic or a body-centered cubic lattice. Theoretical calculations of Leibler [15] suggest a body-centered arrangement of spheres. However, calculation of volume fractions of domain-forming component from SANS data obtained by us [16] and others [17] suggest, on comparison with volume fractions obtained by analysis, that a face-centered cubic arrangement

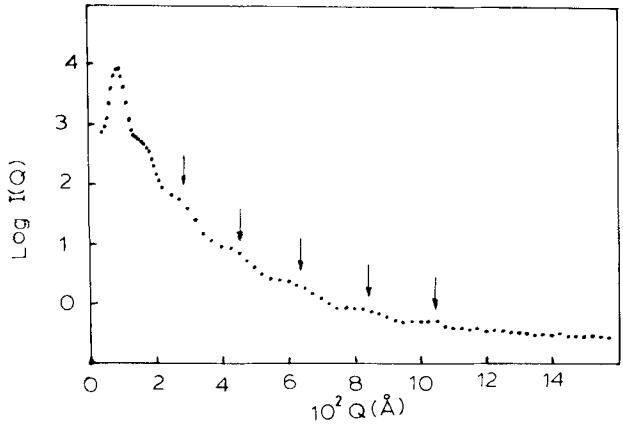

FIG. 5. Small-angle neutron scattering from diblock styrene-isoprene copolymer with a deuterostyrene block weight fraction of 0.82 and a total molecular weight of 99 600.

is favored. Values of D as a function of M_D followed the predictions of Eq. (11), but the relation between d and M in no way followed that predicted by Eq. (12). Viscosity effects limiting the attainment of equilibrium separations have been cited as the reason for this observation.

Both Meier's [18] earlier theory of domain formation and Helfand's narrow-interphase approximation theory predict that the boundary between domain and matrix should be diffuse over a finite region. Helfand predicts a constant value for the thickness of this region over all molecular weights, while Meier predicts an increasing thickness as the molecular weight decreases. The extent of this diffuse interface can be observed by SANS, provided that one block is wholly deuterated to increase the contrast factor. This is necessary since the analysis relies on deviations from Porod's law, i.e., for randomly oriented bodies with sharp boundaries, the intensity decays smoothly as Q^{-4} when $DQ >> 1$. Since $D \simeq 100$ Å, Q must be greater than 10^{-2} Å^{-1} in practice, much larger values are required to estimate the incoherent background accurately. In the presence of a diffuse boundary, the intensity decays much faster than Q^{-4} and, after subtraction of background,

$$I(Q) = K_p Q^{-4} \exp(-\sigma^{-2} Q^{-2}), \tag{13}$$

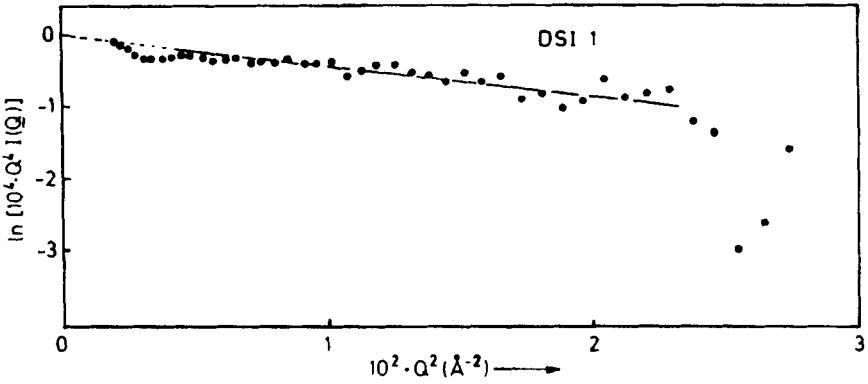

FIG. 6. SANS data plotted according to Eq. (13).

where K_p is the Porod constant, which contains the surface-to-volume ratio of the particle, the contrast factor, and the machine parameters.

The factor σ in Eq. (13) is the second moment of the density distribution (assumed Gaussian) across the interface, which means that the interface thickness is given by $(12)^{1/2}\sigma$. A plot of data according to Eq. (13) is shown [19] in Fig. 6, while Fig. 7 shows the interfacial volume fractions obtained from SANS data compared to theoretical predictions.

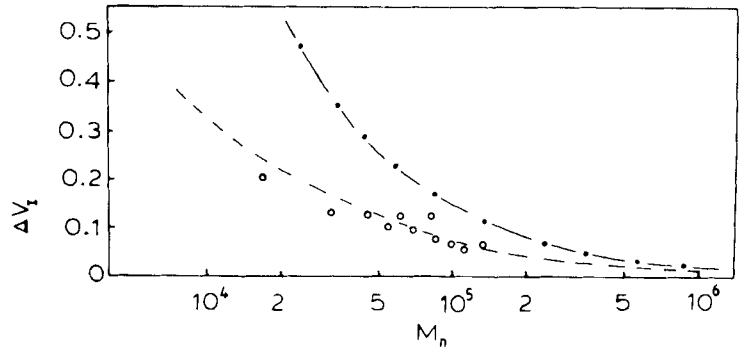

FIG. 7. Interfacial layer volume fraction obtained from SANS data compared to theoretical predictions Helfand (●) and Meier (○).

The small-angle scattering from block copolymers has been modeled by combining expressions for $P(Q)$ and the interfacial contribution with interference-function expressions derived from crystallinity [20]. By introducing distributions to the crystalline lattice and incorporating a dispersion of comain sizes, where there is almost exact agreement with distortions of the second kind, i.e., the domains are effectively arranged on a paracrystalline lattice.

KINETICS OF MICROPHASE SEPARATION

At sufficiently high temperatures, block copolymers, like homopolymer mixtures, become homogeneous. However, on cooling the block copolymer melt, the kinetics and thermodynamics of the phase-separation process differ from those of homopolymers due to the connections between the blocks. Leibler used the random-phase approximation to obtain the expression in terms of an order parameter describing the average deviation of segment density from the average density. By this means, Leibler [15] predicts that only three equilibrium microphase-separated structures are permissible: body-centered cubic spheres, hexagonally packed cylinders, or alternating lamellae.

In the homogeneous disordered state, the scattering law obtained for a linear diblock copolymer with A and B blocks is given by

$$S(Q) = [(F(u)/N) - 2\chi]^{-1}, \tag{14}$$

where χ is the Flory-Huggins interaction parameter between the two block forming polymers, u is equal to $Q^2\langle S^2\rangle$, N is the degree of polymerization of whole molecules, and

$$F(u) = g(1,u)/\ g(\phi_B,u) - \frac{1}{4}[g(1,u) - g(\phi_A,u) - g(\phi_B,u)]^2 \ ,$$

where

$$g(\phi,u) = 2(\phi u + \exp(-\phi u) - 1)/u^2 .$$

Equation (14) has a maximum at a finite value of Q (Q_{max}). The value of Q_{max} is determined by the value of $\langle S^2\rangle$, while the amplitude and breadth of the peak is determined by the product χN. The scattering will increase as the temperature is reduced, becoming infinite at the spinodal point, i.e., where phase separation is spontaneous. At this point

$$F(u) = \chi N,$$

and hence, the value of the critical parameter, χN_c, for spontaneous phase separation can be calculated as a function of the volume fraction composition of the copolymer. For $\phi = 0.5$, $\chi N_c = 10.5$. It should be noted that a transformation to the ordered microphase-separated state takes place before the spinodal curve is crossed. Hashimoto [21] outlined a phenomenological Ginzburg-Landau theory of the evolution of the order parameter on the sudden transformation of the copolymer to a new equilibrium state *within* the homogeneous phase. By combining this expression with the random phase approximation developed by Leibler for the free energy of the copolymer melt, the variation of scattered intensity with time, as the system relaxes to its new equilibrium state, is given by

$$I(Q, t) = I(Q, O) \exp(2R(Q)t). \tag{15}$$

The rate constant for the relaxation process, $R(Q)$, is equivalent to the amplification factor in the Cahn-Hilliard theory applied to polymer blends and is given by

$$R(Q) = L_O Q^2 (-(F(u)/N) + 2\chi), \tag{16}$$

where L_O is the Onsager coefficient connecting the diffusive flux of copolymer molecules to the local chemical potential responsible for the growth of density fluctuations in the system.

Unlike Eq. (14), $R(Q)$ in Eq. (15) does not become discontinuous as the spinodal line is crossed. Figure 8 shows the theoretical variation of $I(Q)$ as a function of χN for a linear diblock copolymer with a volume fraction composition of 0.5. The variation of $R(Q)$ as a function of $Q\langle S^2 \rangle^{1/2}$ for various values of χN is shown in Fig. 9. When $R(Q)$ is negative, there will be no growth of the order parameter and the density fluctuations will decay. Figure 9 demonstrates that block copolymers have an upper and lower limit to the range of QR_g where $R(Q)$ is positive, and hence the fluctuation wavelength of the growth-order parameter leading to phase separation.

Time-resolved SANS experiments on diblock copolymers were made and the results compared to theory by Connell and Richards [22]. For these experiments a 70% solution of a deuterostyrene-isoprene block copolymer in cyclohexane was used, so that the order-disorder temperature was reduced to a reasonable value. The solution was first equilibrated at a temperature well above the order-disorder temperature and then quenched by dropping

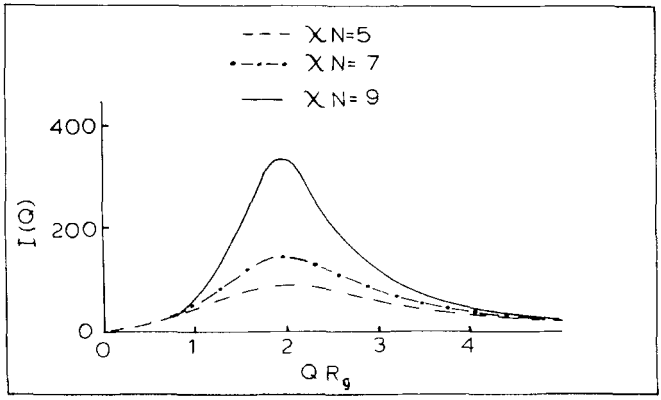

FIG. 8. Variation of scattered intensity as a function of χN for a linear diblock polymer with volume fraction composition 0.5.

the solution into a larger thermostated jacket set at a known lower temperature. After the solution fell into the lower jacket, scattered intensity data were collected for a series of discrete time intervals. Figure 10 shows data collected for such a series of "frames" for one copolymer. Values of $R(Q)$ were obtained by plotting ln $I(Q)$ as a function of time for fixed Q. Figure 11 shows a plot of $R(Q)/Q^2$ as a function of Q^2 and the nonlinear least-squares fit of Eq. (16) to the data. Clearly, there is a lower limit to growth,

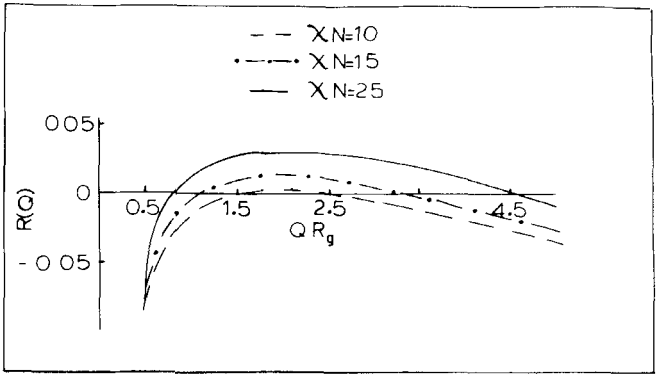

FIG. 9. Variation of $R(Q)$ with χN calculated by Leibler's theory.

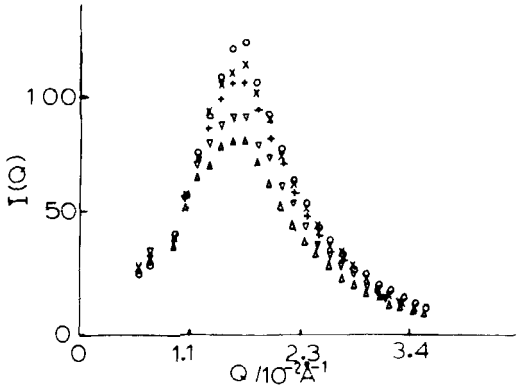

FIG. 10. Time-resolved SANS profiles for deuterostyrene-isoprene, 70% in cyclohexane with temperature quench. Initial temperature 90°C. Quench temperatures: (△) 4°C, (▽) 12°C, (+) 28°C, (X) 44°C, (○) 60°C.

but the data do not show any upper limit. This is attributed to the neglect of random thermal fluctuations first discussed by Cook and the absence of any Q dependence of the Onsager coefficient in our analysis. With values of χ, L_O and R_g obtained from such data, the local thermodynamic driving force and the growth rate of the order parameter can be calculated as a function of Q. Experimental data are compared to theoretical curves in Fig. 12. The

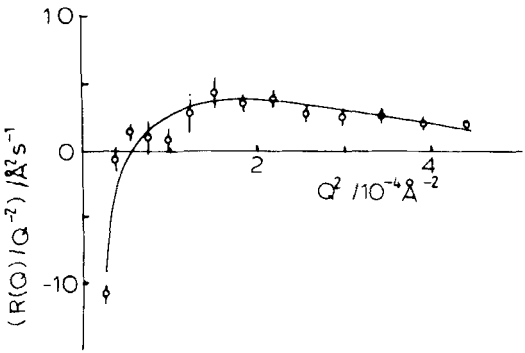

FIG. 11. $R(Q)/Q^2$ as a function of Q^2 from the data of Fig. 10. Solid lines are fits of the theoretical expression to the data.

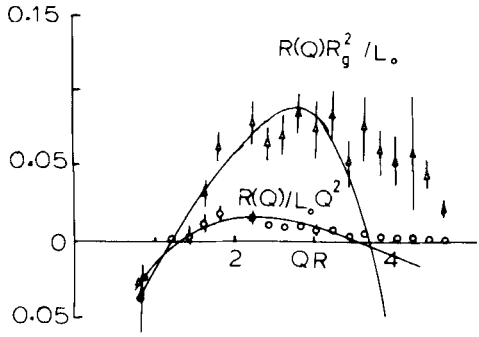

FIG. 12. Fluctuation growth rate $(R(Q)/R^2 L_Q)$ and local thermodynamic driving force for the temperature quench indicated.

disagreement at higher Q is thought to be due to the simplifications adopted in the analysis mentioned earlier.

MOLECULAR DIMENSIONS OF DOMAIN-FORMING BLOCKS

Attempts to obtain the molecular dimensions of blocks in solid copolymers have met with only limited success thus far. Furthermore, the interpretation of the values obtained is unclear due to the distribution in orientation of the domains. Ideally, the radii of gyration normal and parallel to the boundary between domain and matrix are required. Clearly, for spherical domains these two values cannot be separated and a spherically averaged value of R_g is obtained. For lamellar and cylindrical domains, alignment usually necessitates drastic processing, which results in nonequilibrium morphologies.

An additional complication is the strong Bragg scattering in the region where the molecular scattering occurs, which must be removed by some means to obtain artifact-free molecular scattering. Richards and Thomason [23] tried the direct approach of subtracting the scattering of a fully hydrogenous styrene-isoprene copolymer from that of a copolymer containing a few percent of a deuterostyrene-isoprene copolymer. This approach had only limited success. The correct method became apparent with the publication of expressions for the scattering from multicomponent polymer systems by Jahshan and Summerfield [24]. For such systems the scattering law may be written as

$$S(Q) = (x\rho_p{}^D + \rho_p(1-x) - \rho_m)^2 S^T(Q) + x(1-x)(\rho_p{}^D - \rho_p)^2 P(Q)20, \quad (17)$$

where ρ_p is the scattering length density of hydrogenous domain-forming blocks, $\rho_p{}^D$ is the scattering length density of domain-forming block when fully deuterated, ρ_p is the scattering length density of the matrix-forming material, x is the mole fraction of deuterated segments in the domain-forming blocks, $S^T(Q)$ is the combined scattering law for the domain and the interference function, and $P(Q)$ is the single-chain scattering law.

Thus by adjusting x such that

$$x\rho_p{}^D + \rho_p(1-x) - \rho_m = 0,$$

only the single-chain scattering law remains. This technique has been successfully used by Cohen et al. [25] on styrene-butadiene copolymers and by Richards and Qureshi [26] on styrene-ethylene oxide diblock copolymers. Hasegawa et al. [27] attempted to obtain the radii of gyration of blocks in lamellar styrene-diene copolymers by this technique. However, it is evident that their data in the important low-Q region are contaminated by interference-function scattering, and they had to resort to a Guinier plot analysis of data obtained at higher Q values; consequently, the radii of gyration may be subject to some error.

"INTERPENETRATING NETWORKS"

"Interpenetrating polymer networks" (IPNs) are formed when a monomer is polymerized while in intimate contact with a second preformed polymer. Phase separation takes place during polymerization, but the phase-separated zones are not arranged regularly with respect to each other and, moreover, they are highly polydisperse with respect to their dimensions. Much work on these materials has been reported by Sperling and coworkers, and they produced a theory of the size of the guest polymer phase-separated zones and its dependence on the host polymer network crosslink density and the overall composition of the IPN [28].

SANS has been applied to two IPN systems: polystyrene in polydimethylsiloxane (PS/PDMS) and polymethacrylic acid in polydimethylsiloxane (PMAA/PDMS) swollen by water [29]. For both systems the scattering profiles were devoid of distinctive features. For the PS/PDMS IPNs, Porod plots ($Q^4 I(Q)$ vs (Q^2)) were sensibly horizontal over the whole range of Q. On the assumption that the phase-separated PS zones were spherical (i.e., adopting

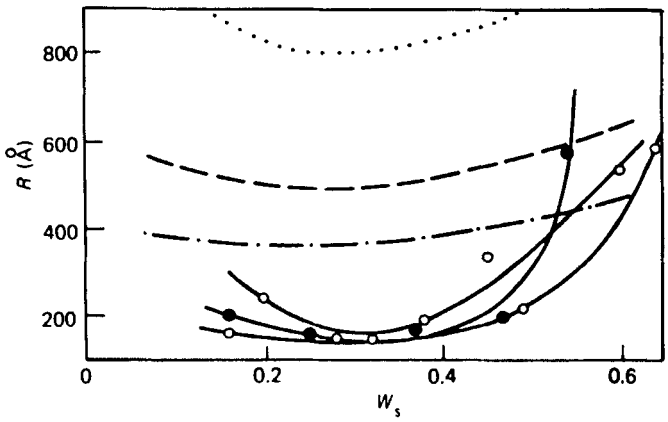

FIG. 13. Radius of polystyrene zones in polydimethylsiloxane-polystyrene interpenetrating networks as a function of styrene weight fraction.

the assumption made by Yeo et al. in their theory), the radii of the zones were calculated from this constant value of $Q^4I(Q)$ since, for spherical particles in the Porod region,

$$Q^4I(Q) = 12\pi D_s T_s K_f^2 \phi_p/(1 - T_w)R, \tag{18}$$

where D_s is the thickness of the IPN specimen, T_s is the neutron transmission of the IPN, T_w is the neutron transmission of water (used as calibrant in SANS experiments), ϕ_p is the volume fraction of guest polymer in the IPN, and R is the equivalent spherical radius of phase-separated zones.

Values of R obtained are compared with the predictions of theory in Fig. 13. There is no influence of host network (PDMS) crosslink density on the radius and, moreover, the experimental values are at least half those theoretically predicted. However, qualitatively the experimental radii do agree with the Yeo theory in that the minimum is observed at a certain composition. Correlation lengths were obtained from Debye plots of the scattered intensities, and the resultant chord lengths in the PSD zones had a curved dependence on PSD content with no apparent minimum.

The analysis using the Porod law and spherical zones in the PSD/PDMS case is applicable when the zones are discrete (or reasonably so). Electron microscopy confirmed this for PSD/PDMS IPNs. For PMAA/PDMS IPNs, electron micrographs gave no indication of discrete PMAA zones, and further-

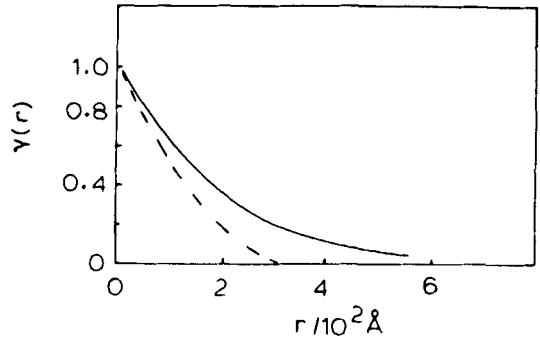

FIG. 14. Correlation function obtained from SANS data for polydimethylsiloxane-poly(methacrylic acid) interpenetrating network swollen in D_2O. Weight fraction of polymethacrylic acid 0.41. Volume fraction of D_2O 0.39.

more, permeation experiments indicated that the PMAA zones were continuous. Consequently, SANS data were analyzed by the statistical methods outlined earlier. To increase the contrast and improve the scattered intensity, the IPNs were swollen to equilibrium in D_2O. Figure 14 shows a typical correlation function obtained for one of the PMAA/PDMS IPNs; the chord length in the D_2O-swollen PMAA zones shows a linear dependence on total volume fraction of phase-separated material. Although the Porod analysis could not be

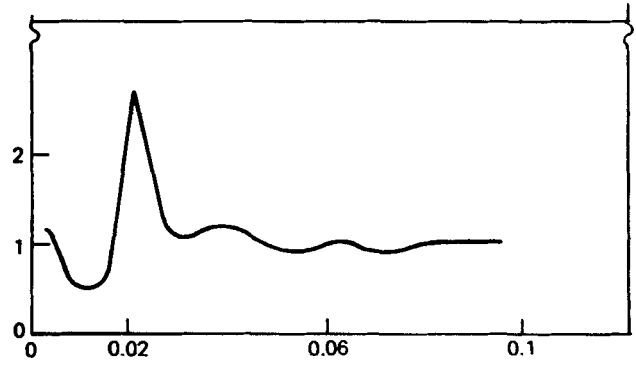

FIG. 15. Structure factor obtained for a polydimethylsiloxane-deuteropolystyrene interpenetrating network. Weight fraction of polydimethylsiloxane 0.28

used to obtain equivalent sphere radii, it was used to obtain the dimensions of the diffuse interfacial region that was evident since the intensity at high Q attenuated at a faster rate than Q^{-4}. Typically diffuse layer thickness values were between 20 and 45 Å. This diffuse layer was interpreted as a region in the PMAA zones where the D_2O concentration fell to zero because the hydrophobic nature of the PDMS matrix is transmitted to some extent into the PMAA zones.

For the PSD/PDMS IPNs an attempt was made to ascertain whether there was any regularity in the separation of the PSD zones. The analysis used was that applied to concentrated colloidal dispersions. Assuming that the PSD zones were spherical, the scattering law for an isolated zone was calculated by fitting Eq. (8) (adjusted for a distribution in zone size) to the experimental scattering data. From the parameters of this fit, $P(Q)$ was calculated over the complete range of Q. This calculated scattering law was then divided into the experimental data to obtain the structure factor describing the arrangement of PSD zones in the IPN. Figure 15 shows one such structure factor obtained, implying some regularity in separation at short distances but a random structure at large length scales.

HOMOPOLYMERS

One of the important uses of SANS for homopolymers has been the confirmation of the rotational isomeric state theory of polymer configuration. This relies on the ability of SANS to probe length scales down to ~20 Å. Notable work on this aspect of confirmation studies was reported by Flory and coworkers [30] and Fischer et al. [31]. A recent study on these lines, which deserves particular note, is that of Rawiso [32] on polystyrene molecules whose monomer units were deuterium-labeled at different parts. Scattering laws for the backbone, phenyl ring, and worm like chain were evaluated, and the influence of molecular weight polydispersity and chain cross section considered.

Mention should also be made of the studies of transesterification in polyethylene teraphthalate (PET). During attempts to perform SANS measurements on mixtures of deuterated PET in hydrogenous PET obtained by melt processing, it was found that the PET molecules decomposed and recombined in a scrambled manner. Attempts have been made to overcome this effect, and it has been specifically investigated by SANS to ascertain the kinetics of the process [33]. This phenomenon should be foremost in the design of SANS experiments on the new main-chain liquid-crystal polymers.

A continuing major problem in the molecular physics of polymers is presented by the conformational changes that take place when a macromolecule crosslinked into a network is deformed by a bulk network deformation. In principle, SANS is the ideal technique to obtain the necessary data to compare with theoretical predictions. Essentially there are two extreme theories: (1) A junction affine model [34] where the end-to-end distance between topologically connected crosslinks changes to the same extent as the bulk dimensions. (2) The phantom-chain model [35] views the crosslinks as having a random diffusive motion about their mean positions which leads to non-affine network chain dimensions. Attempts to incorporate the essential features of both theories have been made by other workers, notable Flory [36].

Considerable SANS work has been reported by the Strasbourg group [37-39] for anionically prepared end-linked networks. For uniaxially stretched networks a variety of behavior of the chain dimensions with bulk dimensions was observed. Unfortunately, no clear evidence supporting either theory was obtained. A major practical problem with uniaxial extension of networks is the anisotropic nature of the scattering signal obtained. This severely limits the range of Q values usable for obtaining the radius of gyration. In common with others, work in this laboratory [40] used networks that were *swollen* by a solvent to investigate molecular deformation. The scattering from solvent-swollen systems now becomes isotropic. Mixtures of deuteropolystyrene (PSD) and hydrogenous polystyrene (PSH) were crosslinked by γ-irradiation of compression-molded specimens. The networks were then swollen to equilibrium in toluene at 293 K and in cyclohexane at a range of temperatures up to 338 K. Zimm plots for a range of PSD concentrations showed that the second virial coefficient was zero and the molecular weights of the labeled species obtained from SANS data were in good agreement with the previously determined GPC values. However, dry unswollen specimens usually showed enhanced low-Q scattering which varied randomly from specimen to specimen. This extra scattering could only be attributed to microvoids in the specimens even though these samples had been annealed after initial compression molding and, following crosslinking, had been swollen in toluene to extract uncrosslinked material, and then dried slowly. Preparation of void-free plaques of polymers by compression molding is frequently much more difficult than appreciated.

When the specimens were swollen by solvent, there was no evidence of void scattering. Values of the radii of gyration obtained and comparison with phantom chain and affine models are given in Table 3. For all the crosslink densities examined, the data appear to fall between the two models, but attempts to interpret the data by using Ullman's model for randomly cross-

TABLE 3. SANS Data for Polystyrene Networks Swollen to Equilibrium in Toluene and Cyclohexane

Swelling ratio	$\langle S^2 \rangle^{1/2}$, Å	$\langle S^2 \rangle z/\langle S^2 \rangle_0$		
		Measured	Phantom	Affine
		Toluene at 293 K		
8.5	155	2.8	2.5	3.5
11.3	152	2.7	1.6	4.0
11.6	158	2.9	2.3	3.8
14.9	156	2.8	2.3	2.9
23.9	151	2.6	2.4	3.8
		Cyclohexane at 308 K		
2.9	95	1.0	1.5	1.8
3.5	116	1.6	1.5	2.0
3.8	95	1.0	1.5	2.0
4.3	112	1.4	1.4	2.1
5.0	112	1.4	1.4	2.1
4.9	92	1.0	1.4	2.1
6.0	113	1.5	1.4	2.4

linked networks fared no better. An additional perplexing feature was the temperature dependences of the labeled, randomly crosslinked chain in cyclohexane-swollen networks. The data reported in Table 3 were obtained from networks crosslinked to different extents to promote a range of volumetric swelling. It was reasoned that, by using one network swollen at different temperatures in one solvent, any artifacts due to an increasing number of crosslinks could be avoided. The results are shown in Table 4. The bulk swelling increases monotonically, but the radii of gyration go through a maximum. Although various possible causes of this behavior were reviewed, they were all rejected. Similar behavior has *not* been observed for homopolysty-

TABLE 4. Influence of Temperature on Radius of Gyration of Labeled Chain in a Cyclohexane Swollen Network

Temperature, K	Swelling ratio	$\langle S^2 \rangle^{1/2}$, Å
308	4.9	92
313	5.6	110
318	6.2	125
325	6.9	123
333	7.7	113
338	8.0	66

rene over the same temperature range. Perhaps the only clear conclusion from this and all other experimental SANS work on networks is that more questions have been raised than answered.

Before closing this section, we return to a basic aspect of SANS experiments on polymers. Contrast, and hence scattered intensity, is generated due to the difference in scattering-length density differences between hydrogenous and deuterated polymer. Whether low or high levels [41] of labeled polymer are used in the experiment, a fundamental assumption is that deuterium labeling does not substantially modify the thermodynamic properties of the polymers. Recent work by Bates [42, 43] calls this assumption into question. In a series of light-scattering and SANS experiments on mixtures of deuterated and hydrogenous butadienes, the scattering data were fitted by the random phase expressions only by adopting small but positive values for the polymer-polymer interaction parameter, χ, rather than the ideal mixing value of $\chi = 0$. Similar results were found for mixtures of deuterated and hydrogenous styrene. In each case, values of χ were obtained by using this parameter as the only adjustable quantity in the fitting procedure, and furthermore, the molecular weights involved were rather high, ranging from 200 000 to 500 000. Stein and coworkers [44] have obtained a very much smaller value of χ by SANS for mixtures of deuterated and hydrogenous polystyrene. As a consequence, this aspect of homopolymer compatibility is still a subject of much discussion.

MACROMOLECULAR MONOLAYERS

The most recent application of neutron scattering has been the measurement of the intensity of neutrons reflected from surfaces. Materials thus far investigated include magnetic materials, superconductors, thin films deposited on surfaces, low-molecular-weight monolayer-forming materials, surfactants, and polymers in solution. The technique was first demonstrated some 12 years ago by Hayter, Penfold, and Williams [45], while Thomas [46-48] at Oxford has developed both x-ray and neutron reflectometry from liquid surfaces.

In a collaboration with the group at Oxford, a program of research on the structural physics of polymers spread at air-liquid interfaces has been initiated [49]. For a beam of neutrons of wavelength λ, the refractive index of any substance for the neutron beam is given by

$$n = 1 - \frac{\lambda^2 \rho}{2\pi} - \frac{iN\lambda^2 \sigma_A}{4\pi^2}, \tag{19}$$

where N is the number of nuclei per cm^3 and σ_A is the adsorption cross section. For most materials σ_A is 0. Consequently, from Eq. (19), since for air $\rho = 1$, liquid phases will have a smaller refractive index. Total reflection of the incident beam takes place when the incident angle is less than some critical value, θ_c, defined by

$$\cos \theta_c = n_2/n_1,$$

where n_1 and n_2 are the refractive indices of the air phase and liquid phase, respectively. For angles greater than θ_c, partial refraction takes place from each interface in the separating bulk liquid from air. The reflectivity profile, i.e., the reflected neutron intensity as a function of the scattering vector Q, can be calculated by optical matrix methods [50] and may be compared with the experimental data. Essentially, the reflectivity profile corresponds to the scattering length-density profile normal to the interface between the air and liquid phases. Consequently, the thickness and composition of any thin film, be it a diffuse or sharp boundaried layer, can be determined.

Diblock copolymers of styrene and ethylene oxide have been investigated spread as monolayers of increasing surface concentration at an air-water inter-

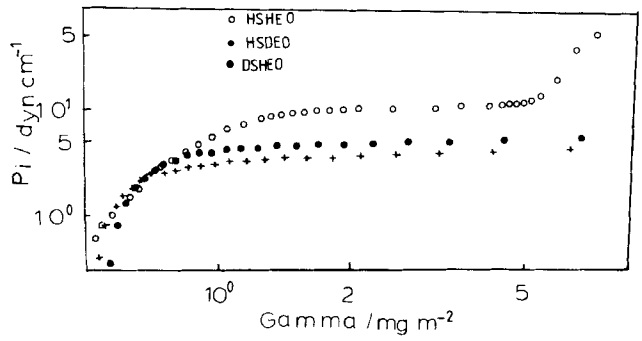

FIG. 16. Surface pressure as a function of surface concentration for linear styrene-ethylene oxide diblock copolymers at the air-water interface.

face. The variation of surface pressure with surface concentration is shown in Fig. 16, while Fig. 17 shows reflection profiles for a fully hydrogenous copolymer spread on D_2O. The solid lines are fits to the data for the polymer layer modeled as a solid slab. Some values of the layer thickness and composition are given in Table 5. Overall, the picture seems to be that the polystyrene block forms a very thin layer which contains water, while the polyethylene oxide block is solvated in the aqueous subphase. As the surface concentra-

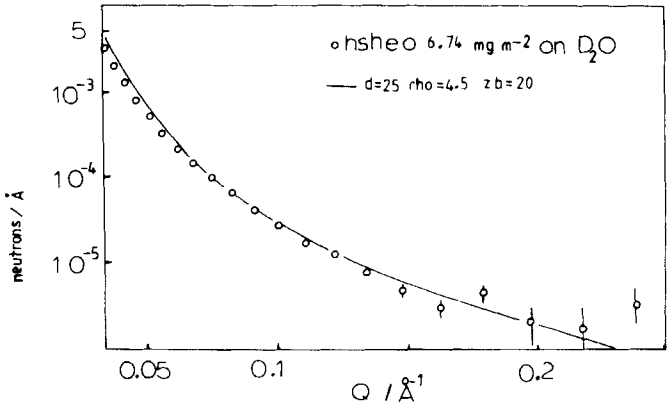

FIG. 17. Neutron reflectivity profile for a fully hydrogenous styrene-ethylene oxide diblock copolymer at the D_2O-air interface.

TABLE 5. Values of Scattering Length Density, Layer Thickness, and Water Content for Hydrogenous Styrene-Ethylene Oxide Block Copolymers Spread on D_2O

Surface concentration, mg/m^2	Scattering length density, ρ, $Å^{-2}$	Layer thickness, t, Å	Water content, % D_2O
0.77	1.2	20	-0.12[a]
1.53	1.8	24	0.01
2.6	2.4	28	0.14
5.49	2.7	42	0.2

[a]This negative value of D_2O content is thought to be due to the preferential incorporation of the H_2O present in D_2O due to exchange with the atmosphere.

tion increases, water is rejected from the polystyrene layer, and the polyethylene oxide layer becomes more dilute and stretches further into the aqueous subphase. More detailed experiments have been performed by using partially deuterated polymers and by varying the contrast by employing subphases of differing ratios of H_2O to D_2O. These data are in the process of being analyzed.

REFERENCES

[1] R. W. Richards, in *Developments in Polymer Characterisation*, Vol. 5 (J. V. Dawkins, ed.), Applied Science Publishers, 1985, Chap. 1.
[2] G. D. Wignall, in *Encyclopedia of Polymer Science and Engineering*, 2nd ed., Wiley-Interscience, New York, To Be Published.
[3] J. S. Higgins, in *Treatise on Materials Science and Technology*, Vol. 15, *Neutron Scattering* (G. Kostorz, ed.), Academic, New York, 1982.
[4] R. Ullman, *Annu. Rev. Mater. Sci.*, *10*, 261(1985).
[5] W. Marshall and S. W. Lovesey, *Thermal Neutron Scattering*, Oxford University Press, 1971.
[6] S. W. Lovesey, *Theory of Neutron Scattering from Condensed Matter*, Oxford University Press, 1984.

[7] G. Kostorz, in *Treatise on Materials Science and Technology*, Vol. 15, *Neutron Scattering* (G. Kostorz, ed.), Academic, New York, 1982.
[8] W. Burchard, *Adv. Polym. Sci., 48,* 1 (1983).
[9] P. W. Debye, *J. Phys. Colloid Chem., 51,* 98 (1947).
[10] R. Ullman, *J. Polym. Sci., Polym. Lett. Ed., 21,* 521 (1983).
[11] Lord Rayleigh, *Proc. R. Soc., London, A90,* 219 (1914).
[12] P. Debye and A. M. Bueche, *J. Appl. Phys., 28,* 679 (1944).
[13] R. W. Richards, *Adv. Polym. Sci., 71,* 1 (1985).
[14] E. Helfand and Z. R. Wasserman, *Macromolecules, 13,* 994 (1980).
[15] L. Leibler, *Macromolecules, 13,* 1602 (1980).
[16] R. W. Richards and J. L. Thomason, *Ibid., 16,* 982 (1983).
[17] F. S. Bates, R. E. Cohen, and C. V. Berney, *Ibid., 16,* 1101 (1983).
[18] D. J. Meier, *Polym. Prepr., 15,* 171 (1974).
[19] R. W. Richards and J. L. Thomason, *Polymer, 24,* 1089 (1983).
[20] R. W. Richards and J. L. Thomason, *Macromolecules, 18,* 452 (1985).
[21] T. Hashimoto, *Ibid., 20,* 465 (1987).
[22] J. G. Connell and R. W. Richards, *Polymer Motion in Dense Systems,* Springer, To Be Published.
[23] R. W. Richards and J. L. Thomason, *Polymer, 24,* 581 (1981).
[24] S. N. Jahshan and G. C. Summerfield, *J. Polym. Sci., Polym. Phys. Ed., 18,* 1859 (1980).
[25] F. S. Bates, C. V. Berney, R. E. Cohen, and G. D. Wignall, *Polymer, 24,* 519 (1983).
[26] M. S. Qureshi and R. W. Richards, Work in Progress.
[27] H. Hasegawa, H. Tanaka, T. Hashimoto, and C. C. Han, *Macromolecules, 20,* 2120 (1987).
[28] J. K. Yeo, L. H. Sperling, and D. A. Thomas, *Polymer, 24,* 307 (1983).
[29] B. McGarey and R. W. Richards, *Ibid., 27,* 1315 (1986); *Br. Polym. J., 19,* 111 (1987).
[30] H. Hayashi, P. J. Flory, and G. D. Wignall, *Macromolecules, 16,* 1328 (1983).
[31] W. Gawrisch, M. F. Brereton, and E. W. Fischer, *Polym. Bull., 4,* 1 (1981).
[32] M. Rawiso, R. Duplessix, and C. Piert, *Macromolecules, 20,* 630 (1987).
[33] J. Kugler, J. W. Gilmer, D. Wiswre, H. G. Zachmann, K. Hahn, and E. W. Fischer, *Ibid., 20,* 1116 (1987).
[34] F. T. Wall, *J. Chem. Phys., 11,* 527 (1943).
[35] H. M. James and E. Guth, *J. Polym. Sci., 4,* 153 (1949).
[36] P. J. Flory and B. Erman, *J. Polym. Sci., Polym. Phys. Ed., 22,* 49 (1984).

[37] M. Beltzung, C. Picot, P. Rempp, and J. Hertz, *Macromolecules, 15,* 1594 (1982).
[38] M. Beltzung, C. Picot, and J. Herz, *Ibid., 17,* 663 (1983).
[39] M. Beltzung, J. Herz, and C. Piecot, *Ibid., 16,* 580 (1983).
[40] N. S. Davidson and R. W. Richards, *Ibid., 19,* 2576 (1986).
[41] A. Z. Akcasu, G. C. Summerfield, S. N. Jahnshan, C. C. Han, C. Y. Kim, and H. Yu, *J. Polym. Sci., Polym. Phys. Ed., 18,* 863 (1980).
[42] F. S. Bates and G. D. Wignall, *Phys. Rev. Lett., 57,* 1429 (1986).
[43] F. S. Bates, S. B. Dierker, and G. D. Wignall, *Macromolecules, 19,* 1938 (1986).
[44] H. Yang, R. S. Stein, C. C. Han, B. J. Bauer, and E. J. Kramer, *Polym. Commun., 27,* 132 (1986).
[45] J. B. Hayter, J. Penfold, and W. G. Williams, *Nature, 262,* 569 (1976).
[46] J. B. Hayter, R. R. Highfield, B. J. Pullman, R. K. Thomas, A. T. McMullen, and J. Penfold, *J. Chem. Soc., Faraday Trans. I, 77,* 1437 (1981).
[47] J. E. Bradley, E. M. Lee, R. K. Thomas, A. J. Willatt, J. Penfold, R. C. Ward, D. P. Gregory, and W. Waschkowski, *Langmuir,* Submitted.
[48] T. L. Crowley, R. K. Thomas, and A. J. Willatt, To Be Published.
[49] R. W. Richards and R. K. Thomas, Work in Progress.
[50] M. Born and E. Wolf, *Principles of Optics,* 6th ed., Pergamon, 1980.

Received April 25, 1988